



Review in Advance first posted  
online on January 3, 2017. (Changes  
may still occur before final  
publication online and in print.)

# Structural Studies of Amyloid Proteins at the Molecular Level

David S. Eisenberg and Michael R. Sawaya

Howard Hughes Medical Institute and Molecular Biology Institute, University of California,  
Los Angeles, California 90095-1570; email: david@mbi.ucla.edu, sawaya@mbi.ucla.edu

Annu. Rev. Biochem. 2017. 86:3.1–3.27

The *Annual Review of Biochemistry* is online at  
[biochem.annualreviews.org](http://biochem.annualreviews.org)

This article's doi:  
10.1146/annurev-biochem-061516-045104

Copyright © 2017 by Annual Reviews.  
All rights reserved

## Keywords

cryo–electron microscopy, cryo-EM, solid-state nuclear magnetic resonance, ssNMR, X-ray diffraction, polymorphs, amyloid symmetry, steric zipper

## Abstract

Dozens of proteins are known to convert to the aggregated amyloid state. These include fibrils associated with systemic and neurodegenerative diseases and cancer, functional amyloid fibrils in microorganisms and animals, and many denatured proteins. Amyloid fibrils can be much more stable than other protein assemblies. In contrast to globular proteins, a single protein sequence can aggregate into several distinctly different amyloid structures, termed polymorphs, and a given polymorph can reproduce itself by seeding. Amyloid polymorphs may be the molecular basis of prion strains. Whereas the Protein Data Bank contains some 100,000 globular protein and 3,000 membrane protein structures, only a few dozen amyloid protein structures have been determined, and most of these are short segments of full amyloid-forming proteins. Regardless, these amyloid structures illuminate the architecture of the amyloid state, including its stability and its capacity for formation of polymorphs.

## Contents

THE AMYLOID STATE .....	3.2
PROTEINS THAT CONVERT TO THE AMYLOID STATE .....	3.5
Pathogenic Proteins .....	3.5
Denatured Proteins .....	3.6
Functional Proteins .....	3.7
METHODS TO LEARN THE MOLECULAR STRUCTURES OF PROTEINS IN THE AMYLOID STATE AND THEIR LIMITATIONS .....	3.7
X-Ray and Electron Diffraction .....	3.7
Solid-State Nuclear Magnetic Resonance .....	3.8
Cryo-Electron Microscopy .....	3.9
SPINES OF AMYLOID FIBRILS .....	3.9
Structural Origin of the Stability of Amyloid Fibrils .....	3.9
SYMMETRY IN AMYLOID ASSEMBLY .....	3.10
Four Basic Sheet Geometries .....	3.10
Ten Symmetry Classes .....	3.12
Strand Registration .....	3.12
THE SEQUENCE DEPENDENCE OF AMYLOID FIBRILS .....	3.14
STRUCTURAL STUDIES OF SOME PATHOGENIC AMYLOID FIBRILS .....	3.14
$\beta$ -Amyloid <sub>1-40</sub> .....	3.14
$\beta$ -Amyloid <sub>1-42</sub> .....	3.16
$\alpha$ -Synuclein .....	3.17
STRUCTURAL BASIS OF POLYMORPHS AND STRAINS .....	3.18
Structural Basis of Seeding and Prion-Like Spreading .....	3.19
STRUCTURAL STUDIES OF AMYLOID OLIGOMERS .....	3.20
SUMMARY AND GAPS IN OUR UNDERSTANDING OF AMYLOID STRUCTURES AT THE MOLECULAR LEVEL .....	3.21

## THE AMYLOID STATE

Amyloid is the term for proteins that form elongated, unbranched fibrils with certain defining properties. Pathologists, who observe such fibrils in diseased brains and other tissues, have traditionally classified protein fibrils as amyloid if they are associated with disease and if they bind the dye Congo red, displaying a green birefringence when viewed between crossed polarizers (1). Protein scientists prefer biophysical definitions because they observe similar fibrils formed both by functional proteins isolated from healthy tissues and by many denatured proteins. The commonly accepted biophysical definition is that amyloid fibrils display the cross- $\beta$  fiber diffraction pattern when examined with X-rays. This pattern was first reported by pioneering biophysicist William Astbury in 1935 (2), who subjected poached egg white to X-rays (**Figure 1**).

From the cross- $\beta$  pattern, Astbury reasoned that protein chains extend perpendicular to the fibril axis and stack together into sheets that lie parallel to each other. A decade and a half later, Pauling & Corey (3) built atomic models of  $\beta$ -sheets on the basis of their crystal structures of small peptides. These models suggested that the extended protein  $\beta$ -strands stacking along the fibril axis are held together by N-H $\cdots$ O=C hydrogen bonds between the backbone amide groups roughly parallel to the fibril direction. Successive amino acid side chains protrude to alternate sides

3.2

Eisenberg • Sawaya



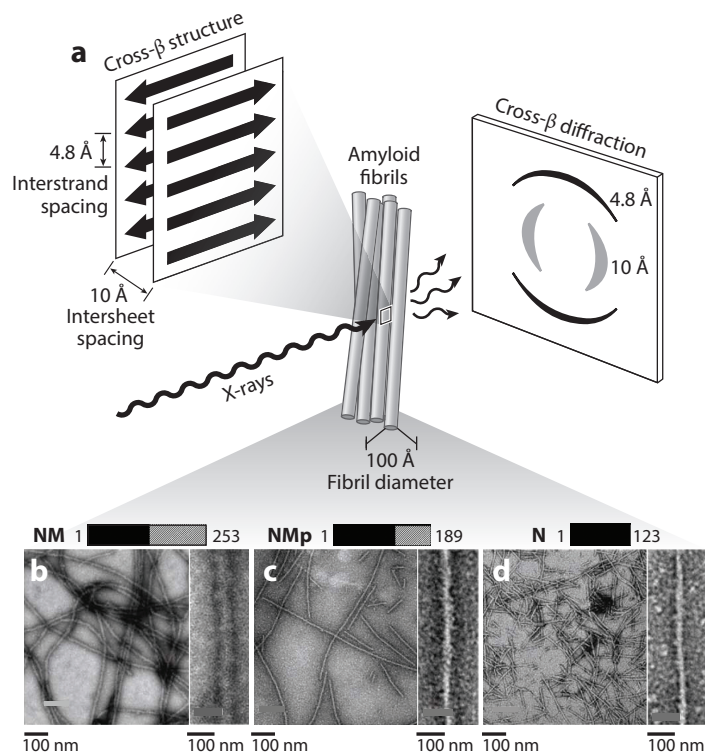
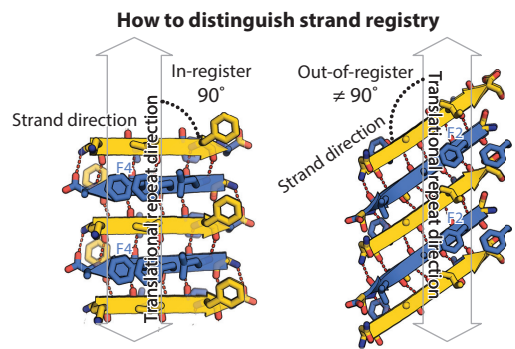
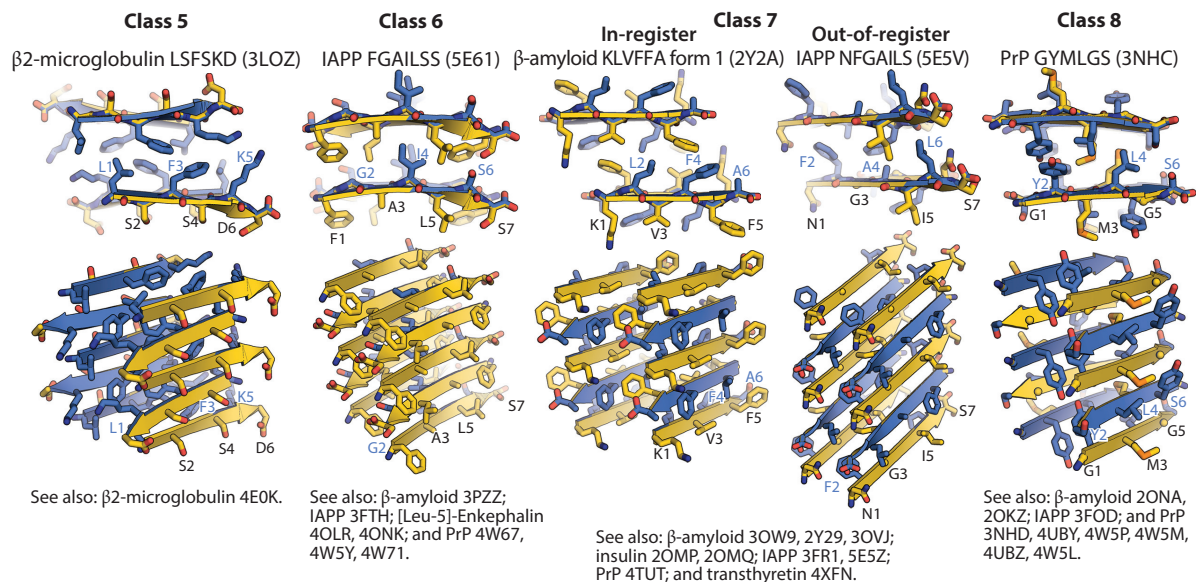
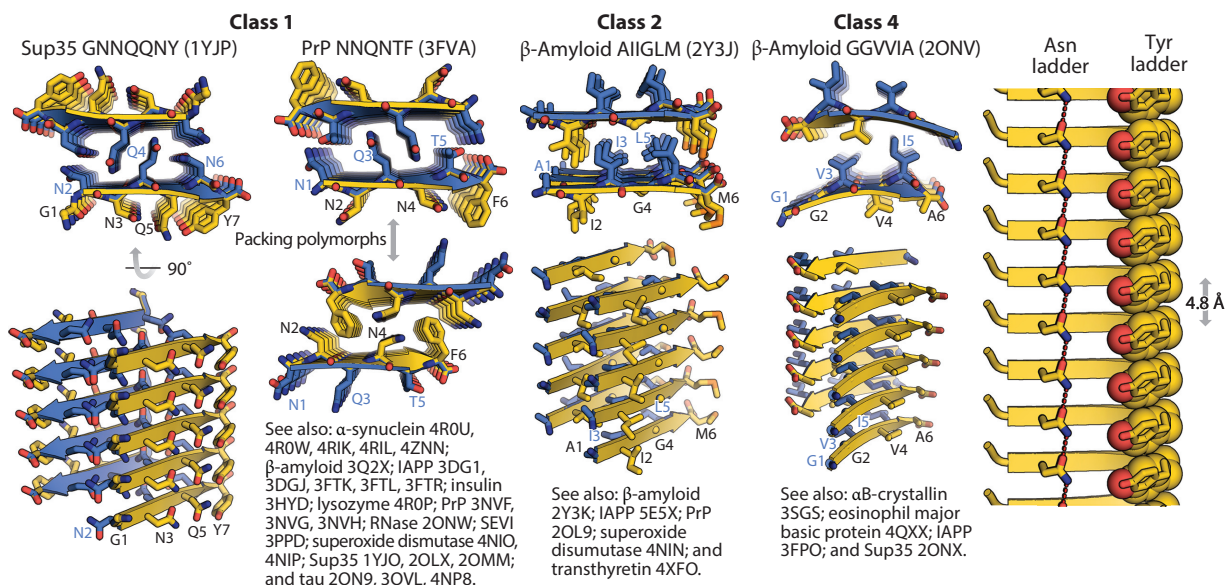


**Figure 1**

The cross- $\beta$  structure of amyloid fibrils. (a) The cross- $\beta$  X-ray fiber diffraction pattern of an amyloid fibril shows two characteristic diffuse reflections. The one at a spacing of 4.8 Å along the vertical axis arises from the stacks of extended  $\beta$ -strands (solid black arrows). The more diffuse reflection at a spacing of  $\sim 10$  Å along the horizontal axis arises from the separation of adjacent  $\beta$ -sheets. (b–d) Electron micrographs of amyloid fibrils formed by various lengths of a yeast prion protein, Sup35. Panels b–d modified from Reference 99 with permission. Notice that (b) the longest segment (containing both N and M domains of Sup35) forms the widest and fuzziest fibrils, (c) the N domain plus partial M domain forms fibrils of intermediate width, and (d) the N domain alone forms the narrowest and smoothest fibrils. This series of micrographs may be interpreted as showing that the fibril spine at the center is the same in all three lengths, with the protein regions outside the spine decorating the periphery. The rectangles above the micrographs show the lengths of the respective segments of Sup35 with their residue numbers.

of the  $\beta$ -sheet. The protein strands forming the  $\beta$ -sheets can run in the same direction (parallel  $\beta$ -sheets) or alternate in opposite directions (antiparallel  $\beta$ -sheets). Thus the model  $\beta$ -sheets of Pauling & Corey defined the bonding between extended protein  $\beta$ -strands within a sheet but not the bonding of  $\beta$ -sheets with one another in amyloid fibrils.

The interactions that bond  $\beta$ -sheets to each other emerged from atomic structures of short fibril-forming segments of amyloid proteins. The first such structure (4) was of a 7-residue segment of a yeast prion, Sup35, shown in **Figure 2**. The  $\beta$ -sheets associate in pairs. The side chains of each member of the pair interdigitate with the side chains of its mating partner sheet. The result is a tight, dry interface. Viewed down the fibril axis, the interdigitating side chains appear like the teeth of a zipper; thus, this motif of a pair of sheets is termed a steric zipper. The tightly mating pair of  $\beta$ -sheets is the protofilament of the amyloid fibrils. Two or more protofilaments twisted together and held by weaker forces form the fibril. Any given amyloid protein can form



Annu. Rev. Biochem. 2017.86. Downloaded from www.annualreviews.org. Access provided by University of California - Los Angeles UCLA on 01/04/17. For personal use only.

fibrils containing various numbers of protofilaments. This phenomenon is one aspect of what is termed amyloid polymorphism. Additionally, the detailed bonding between the two sheets of the steric zipper pair can form in different ways, as described below, thereby increasing the possible number of polymorphs formed by a given amyloid protein. The biological significance of amyloid polymorphism is that it may be the molecular basis of prion strains, also described below.

Even though the proteins that form amyloid fibrils have a great variety of amino acid sequences and biological functions, the fibril spines share common features. This was clear as early as 1959 when Cohen & Calkins (5), examining diseased tissues from various origins by electron microscopy, reported similar elongated, unbranched fibrils. We now know that the widths of amyloid fibrils can vary from approximately 8 nm to more than 20 nm, depending on the size of the protein and the number of protofilaments in the fibrils. By 1968 an X-ray diffraction study revealed that disease-related fibrils are of Astbury's cross- $\beta$  type (6), and in 1997 a synchrotron X-ray study showed that amyloid fibrils of six different proteins, associated with six different clinical syndromes, exhibit the same cross- $\beta$  diffraction pattern (7). Hence, this characteristic diffraction pattern became the defining biophysical feature of amyloid.

**Polymorphs:**  
distinctly different amyloid structures adopted by a single sequence

## PROTEINS THAT CONVERT TO THE AMYLOID STATE

### Pathogenic Proteins

By microscopic examination of tissues from diseased patients, pathologists have found that amyloid fibrils are associated with dozens of serious diseases. **Table 1** lists a sample of these diseases and the particular proteins found as amyloid fibrils. Generally there is a one-to-one relationship of protein to disease, but in the case of Alzheimer disease, amyloid fibrils of two proteins are found in brain tissues. These are A $\beta$  ( $\beta$ -amyloid) and Tau. Fibrils of A $\beta$  are found in the extracellular plaques first described by Alois Alzheimer in 1907, and fibrils of Tau are found in intracellular tangles, also described by Alzheimer. Whereas fibrils of A $\beta$  are seen only in Alzheimer disease, fibrils of Tau are associated with some two dozen clinically distinct pathologies, three of which are listed in **Table 1**: Alzheimer, Pick, and chronic traumatic encephalopathy, commonly termed CTE (the condition athletes apparently develop from concussive blows to the head).

The extent to which amyloid fibrils cause these diseases is a matter of intense scientific investigation. For several of these diseases there is strong evidence that the aggregating protein is the cause, but the question remains about the particular aggregating state of the protein that is causal. For example, families afflicted by Alzheimer disease at an early age have been identified. Each

←

### Figure 2

A selection from 77 published crystal structures of amyloid steric zippers, with views both parallel to the fibril axes (showing the interdigitation of side chains) and perpendicular to the fibril axes (showing 5 of the  $\sim 50,000$  layers of  $\beta$ -strands in actual fibrils of the 2  $\beta$ -sheets). The steric zippers are organized into symmetry classes, depending on the relative orientations of the two sheets of the steric zipper pair. Representatives of the seven observed symmetry classes are shown, labeled by the parent amyloid protein and segment sequence. The remaining class members are listed by Protein Data Bank identification code. Each strand has a face (*blue*) and a back (*gold*). A reference strand is indicated by labeled residue names and numbers. Reference strands have the same orientation in each class to facilitate comparison of symmetry elements. Oxygen atoms are red; nitrogen atoms are blue. Parallel in-register sheets are capable of forming energetically favorable ladders, such as the asparagine (Asn) and tyrosine (Tyr) ladders from GNNQQNY illustrated in the upper right corner. A means of determining whether a sheet is in-register or out-of-register is depicted for Class 7. If the direction of translational repeat (*white vertical arrows*, drawn to connect identical residues from identically oriented strands) is orthogonal to the strand direction, the sheet is in-register. If the angle is not orthogonal, the sheet is out-of-register. Abbreviations: IAPP, islet amyloid polypeptide; PrP, prion protein; RNase, ribonuclease; SEVI, semen-derived enhancer of viral infection; Sup35, yeast prion and translation release factor.

**Table 1** Some amyloid-related diseases and the associated protein in the amyloid state

Disease	Protein fibril(s)
Alzheimer disease	$\beta$ -Amyloid, Tau
Parkinson disease	$\alpha$ -Synuclein
Diabetes type 2	Islet amyloid polypeptide (aka amylin)
Light chain amyloidosis	Immunoglobulin G light chains
Senile amyloidosis	Transthyretin
Insulin amyloidosis	Insulin
Amyotrophic lateral sclerosis (Lou Gehrig disease)	SOD1, TDP-43, C9orf72, and other proteins.
Chronic traumatic encephalopathy	Tau
Pick disease	Tau
Huntington disease	Huntingtin
Some cancers	p53
Kidney dialysis amyloidosis	$\beta_2$ -microglobulin
Creutzfeldt-Jakob disease, Gerstmann-Sträussler-Scheinker syndrome, kuru, fatal familial insomnia	PrP
Bovine spongiform encephalopathy, variant Creutzfeldt-Jakob disease (aka mad cow)	PrP
Chronic wasting disease (elk, deer, and moose)	PrP
[Psi+] yeast phenotype	Sup35
[Ure2] yeast phenotype	Ure3

Abbreviations: IAPP, islet amyloid polypeptide; PrP, prion protein; SOD1, superoxide dismutase 1; TDP, TAR DNA-binding protein 43.

family has been found to carry a mutation either in the enzyme presenilin that cleaves one end of A $\beta$  from the amyloid precursor protein (APP), or in APP itself, thereby increasing the amount of A $\beta$  (8, 9). When these mutant proteins are overexpressed in experimental animals, the animals show the hallmark plaques. Such experiments suggest that high levels of A $\beta$  are a cause of Alzheimer disease, but they do not define the toxic form of A $\beta$ . Serious doubts that the fibrils of A $\beta$  in plaques are disease causing emerged from findings that the number of A $\beta$  plaques in the brain does not correlate to the severity of dementia in patients (10). Postmortem examination shows that some elderly individuals exhibited plaques, but these individuals also demonstrated cognitive performance as high as age-matched controls without pathology (11).

Aggregates smaller than full amyloid fibrils of A $\beta$ , termed oligomers, are now believed by some scientists to be the toxic entities in Alzheimer disease (12–14). However, because of the difficulties in characterizing these transient aggregates, there is little agreement about the structure or even the stoichiometry of oligomers (15, 16). Similar difficulties cloud the identification of the toxic species—either oligomers or fibrils—of Tau also associated with Alzheimer disease, of  $\alpha$ -synuclein associated with Parkinson disease (17, 18), and of islet amyloid polypeptide (IAPP) associated with type 2 diabetes (19) (P. Krotee, J.A. Rodriguez, M.R. Sawaya, D. Cascio, F.E. Reyes, D. Shi, J. Hattne, B.L. Nannenga, M.E. Oskarsson, S. Philipp, S. Griner, L. Jiang, C.G. Glabe, G.T. Westermark, T. Gonen, and D.S. Eisenberg, unpublished manuscript).

### Denatured Proteins

Astbury's experiment with poached egg white can be interpreted as showing that egg albumin denatured by heat converts to the amyloid state. Since then, scientists have found that they can convert many proteins into amyloid fibrils by heat, pH changes, agitation, or chaotropic solvents

Eisenberg • Sawaya



(20, 21). In 1991–1992, two laboratories reported that the transport protein, transthyretin, converts to amyloid fibrils in mildly acid solutions (22, 23). These reports carried medical implications because fibrils of transthyretin are found in several amyloid diseases, and the pH values that produce its conversion to the amyloid state are accessible within lysosomes of cells. Later, Dobson and colleagues extended studies of in vitro conversion to the amyloid state of several proteins commonly studied by biochemists: These included lysozyme (24), an SH2 domain (25), myoglobin (26), and even several homopolymeric peptides, such as polyalanine (27). Still later, a computational, genome-wide study suggested that the vast majority of proteins contain amyloid-prone segments, capable of promoting aggregation to the amyloid state if the native folds of these proteins are destabilized and opened by mutation or partial denaturation (28). This cohort of proteins capable of forming amyloid fibrils is termed the amyloome.

### Functional Proteins

Whereas amyloid proteins were once considered mainly as disease agents, biological scientists are discovering that nature has adapted amyloid fibrils for biological functions in all kingdoms of life (29, 30). A few examples are briefly listed here: (a) On the surface of *Escherichia coli*, the stable but flexible curli are amyloid fibrils (31). (b) In our pituitary secretory granules, some 24 different peptide hormones are stored in the amyloid state (32). (c) In melanocytes of skin, the protein Pmel17 functions in an amyloid fibril (33). (d) In the protein- and RNA-rich stress granules of higher cells, the low complexity domains of RNA-binding proteins form amyloid-like fibrils (34). (e) In brains, an amyloid-forming protein is involved in the formation of long-term memories (35). (f) Additionally, amyloid fibrils are now being engineered to carry out a variety of planned functions (36, 37).

## METHODS TO LEARN THE MOLECULAR STRUCTURES OF PROTEINS IN THE AMYLOID STATE AND THEIR LIMITATIONS

### X-Ray and Electron Diffraction

Given well-ordered crystals, these diffraction methods can yield accurate structures at atomic resolution, with virtually no prior assumptions about the arrangement of atoms. The challenge presented by amyloid fibrils is that their twisting architecture does not lend itself to forming crystals, because crystals must have translational symmetry. Overcoming this challenge, Balbirnie et al. (38) discovered that short segments of amyloid-forming proteins can themselves form both amyloid fibrils and closely related crystals. They crystallized a seven-residue segment of the amyloid-forming protein Sup35 with sequence GNNQQNY. This segment was identified by searching for the shortest segment of Sup35 that in isolation from the rest of the protein could form an amyloid fibril. The catch with these crystals is that they are micron sized (see the sidebar titled Microcrystals of Amyloid), and it took five years from their discovery until the development of synchrotron X-ray microbeams sufficiently focused and intense to determine a structure from a single crystal (Figure 2) (4). In these crystals, the amyloid protofilament consists of two flat  $\beta$ -sheets mating as a steric zipper and extending throughout the length of the crystal, some 50,000 layers of short segments.

On the basis of this initial atomic structure of amyloid, the 3D Profile Method (39) identified amyloid-forming segments in other proteins, enabling crystal growth and structure determination (28, 40; see also <http://services.mbi.ucla.edu/zipperdb/>). The identified segments invariably form amyloid fibrils in vitro, and in almost all cases, also form microcrystals. To date, more than



## MICROCRYSTALS OF AMYLOID

The refusal of amyloid crystals to grow larger than micron sized may be a consequence of a strain that builds up as the crystal grows. The strain arises because the  $\beta$ -sheets are clamped flat in the crystal lattice, whereas  $\beta$ -sheets in all globular proteins have a natural twist. This hypothesis for the size limitation of amyloid crystals is strengthened by the finding that longer segments of amyloid-forming proteins, such as the 11-residue NACore segment of  $\alpha$ -synuclein, form even smaller crystals. In this case the crystals are only a few hundred nanometers in cross section, and hence are invisible by optical microscopy. Although these crystals are too small for manipulation and mounting for X-ray analysis, they are an ideal size for microelectron diffraction, and their structure was determined by this frontier method (82).

100 atomic-resolution amyloid structures have been determined from some 15 disease-associated proteins (41–51). In every case, the structure found is a steric zipper. Other algorithms for prediction of aggregation are available, and several have been compared and evaluated (52).

The information these segment structures offer about full amyloid fibrils is limited. The fibrils formed by some segments may represent the spines of polymorphs of full fibrils, but others may not. And because the crystallized segment is only a few residues in length, nothing is revealed about the fibril structure outside the spine. Of course, given that the spine probably accounts for much of the energy of aggregation of monomers into the fibril, the spine is an informative segment of the fibril. Another limitation of X-ray structures of steric zipper spines is that, in most cases, they show only the interactions of a segment of one molecule with the identical segment of another molecule; that is, these structures show homo-steric zippers, whereas, as discussed below, hetero-steric zippers formed from  $\beta$ -sheets of two different segments are also important in fibril structures. Despite these limitations, these structures reveal in exquisite detail the atomic factors that account for amyloid structure and stability.

### Solid-State Nuclear Magnetic Resonance

Solid-state nuclear magnetic resonance (ssNMR) has proven to be a powerful method for learning the overall structure of fibrils (53). In this method, amyloid-forming proteins are expressed recombinantly from media containing isotopically labeled amino acids, then fibrils are formed and resonances detected. Much structural information can be extracted from these signals: constraints on the identities of residues, recognition of parallel versus antiparallel  $\beta$ -sheets, registration of strands within a sheet, and inter-residue contacts of amino acid side chains. When enough constraints have been collected, molecular models consistent with all of the constraints can be developed. The process of model development is often aided by additional constraints derived from electron microscopy of the same sample. Structural information on amyloid fibrils extracted from diseased brains can be acquired by seeding isotopically labeled recombinant protein with the diseased fibrils. This amplifies the mass of fibrils, thereby producing sufficient amounts of labeled fibrils that are presumed to have the same structure as the brain material (54).

Such ssNMR determined models show the overall conformation of the well-ordered portion of the chain around the protofilament spine. The major limitation of the NMR-constrained models is that they are exactly that: constrained models, only as accurate as the constraints. The question becomes, are there any other models that satisfy the available set of constraints? As the number and accuracy of constraints accumulates, the model is viewed as an increasingly reliable representation of the true structure. A related limitation is that the relative positions of atoms are not as

3.8

Eisenberg • Sawaya



accurately determined as in an atomic-resolution crystal structure, so that understanding function or designing of drugs may be to some extent impaired.

### Cryo-Electron Microscopy

Recent advances in cryo-electron microscopy (cryo-EM) have enabled the method to provide near-atomic-resolution structures of macromolecular complexes without the need for crystals (55). The twist of an amyloid fibril that hinders crystallization aids 3D (three-dimensional) reconstruction of the fibrils by providing views of a variety of orientations of the molecules that form the fibril.

By combining information from several identical fibrils, cryo-EM can yield the overall fibril structure: the number of protofilaments; the degree of twist; and, depending on the number of well-ordered specimens, information on the atomic structure of the fibril. Cryo-EM and crystallography are complementary: Accurate crystal structures of fragments can be fitted into a cryo-EM reconstruction, yielding what is sometimes termed a pseudoatomic model. Rapid advances in the methodology of cryo-EM are facilitating this process.

### SPINES OF AMYLOID FIBRILS

The mating-sheet, steric zipper spine found in amyloid fibrils of Sup35 has subsequently been found in dozens of atomic structures of segments of amyloid-forming proteins (**Figure 2**). These structures share several similar features: (a) Extended segment  $\beta$ -strands stack together by hydrogen bonding of their amide N-H and C=O groups, forming a  $\beta$ -sheet with the strands spaced by 4.8 Å along the axis. The amide groups are dipolar and stack into dipolar lines, pointing either up or down the fibril. (b) Pairs of the  $\beta$ -sheets are tightly bonded by interdigitating or butting amino acid side chains that extend to both sides of the  $\beta$ -sheets. Depending on the lengths of these side chains, the two sheets can be as close as 5 Å or as far apart as 16 Å (27). (c) The amide-containing side chains of glutamine and asparagine can also form hydrogen bonds between layers of the extended protein chains, creating hydrogen-bonded ladders (**Figure 2**). Other side chains that can form ladders between layers include tyrosine (4), serine, and threonine. (d) The interfaces between the two mating sheets are, with few exceptions, devoid of water. Although rare, a few of the paired sheets have hydrogen bonds between them. These shared architectural features account for the common appearance of all amyloid fibrils in electron micrographs.

### Structural Origin of the Stability of Amyloid Fibrils

Most amyloid fibrils are extraordinarily stable protein assemblies, as their persistence in human tissues suggests. Whereas most protein assemblies are broken apart in 2% sodium dodecyl sulfate (SDS), amyloid fibrils mostly resist SDS treatment. In fact, the GNNQQNY fibrils of a known crystal structure were found to dissolve in 0.5 M NaOH, pure formic acid, and 4 M guanidinium but not in 5% SDS, 4 M urea, or milder solvents (38).

The unusual stability of amyloid fibrils arises from the dual  $\beta$ -sheet structure of their spines. Single  $\beta$ -sheets stabilized by backbone hydrogen bonds assemble and disassemble readily, but the interdigitated dual sheets of steric zippers are stabilized by additional forces. The first is the attractive van der Waals energy that results from the tight-fitting steric zipper interface between the sheets (see the sidebar titled Quantitative Measures of Amyloid Stability). The second factor is the mutual polarization of the hydrogen bonded amide groups that run up and down the sheets. A quantum mechanical calculation suggests that the average hydrogen bond energy of  $-9.1$  kcal/mol-per-hydrogen-bond surpasses that in ice ( $-6.7$  kcal/mol-per-hydrogen-bond) (56). A third factor

**cryo-EM:**  
cryo-electron  
microscopy



## QUANTITATIVE MEASURES OF AMYLOID STABILITY

Amyloid fibrils are unusual in that pairs of  $\beta$ -sheets mate more closely than the adjoining surfaces in other protein complexes. Thus, one useful measure of amyloid stability is the solvent-accessible surface area buried at the interface between the mating sheets. This buried area is typically 150–200 Å<sup>2</sup> per pair of  $\beta$ -strands. For the hetero-steric zipper of **Figure 6c**, this area is 224 Å<sup>2</sup>.

is the entropy gain caused by the release of water molecules bound to the inner faces of the  $\beta$ -sheets as they form the zipper. A fourth factor is the ladders of bonding side chains that form on the surfaces of the paired sheets. Together, these factors produce extraordinarily stable fibrils built on steric zipper spines.

An additional useful measure is the closeness of fit of two protein surfaces, the shape complementarity  $Sc$  (57). This number increases from 0 with no complementarity of the two surfaces and approaches 1.0 for atomic surfaces that fit perfectly together. For tightly mating surfaces of proteolytic inhibitor proteins and their cognate proteases,  $Sc$  lies in the range  $0.73 \pm 0.03$  (57), and for antigen–antibody surfaces,  $Sc = 0.66 \pm .02$ . The dry interfaces between the mating  $\beta$ -sheets of amyloid fibrils display comparable or greater values of  $Sc$ . For example,  $Sc = 0.86$  for the homo-steric zipper of the fibrils of GNNQQNY (**Figure 2**).  $Sc = 0.65$  for the hetero-steric zipper shown in the section below on  $\alpha$ -synuclein.

## SYMMETRY IN AMYLOID ASSEMBLY

Symmetry is intrinsic to amyloid assemblies; it is evident by numerous methods of structure determination and at multiple levels of structural organization. The diversity of symmetry patterns observed highlights the need for the systematic classification of these patterns for understanding and communication of amyloid structure.

In contrast to the nonrepetitive  $\beta$ -sheets found in globular proteins, amyloid  $\beta$ -sheets are composed of multiple identical copies of a polypeptide chain, which naturally leads to patterns of symmetry in their assembly. In this section, we enumerate the symmetry patterns possible for the two most elementary levels of amyloid structure: assembly of strands in a sheet (four patterns possible) and pairs of sheets which mate to form a spine (ten symmetry classes possible) (41, 58). Symmetry at higher levels of amyloid organization—between protofilaments—has been observed by cryo-EM in numerous studies, including those of  $\beta_2$ -microglobulin (59), transthyretin segments (60), insulin (61), and the SH3 domain (62); however, given the lack of high-resolution data at this level, we do not attempt to enumerate their possible patterns of association. Lastly, we define strand registry and illustrate the variations it produces on sheet patterns.

### Four Basic Sheet Geometries

Parallel and antiparallel descriptors of  $\beta$ -sheet geometry are familiar to structural biologists; however, these descriptors encompass only half of the symmetry operations possible in amyloid  $\beta$ -sheets. Parallel and antiparallel describe how N-to-C polarities of neighboring strands align in a sheet. Parallel sheets are defined when strands align with the same polarity, yielding N termini on one edge of the sheet and C termini on the opposite edge (i.e., the arrows point in the same direction in **Figure 3a,c**). Conversely, antiparallel sheets are defined when alternate

3.10

Eisenberg • Sawaya



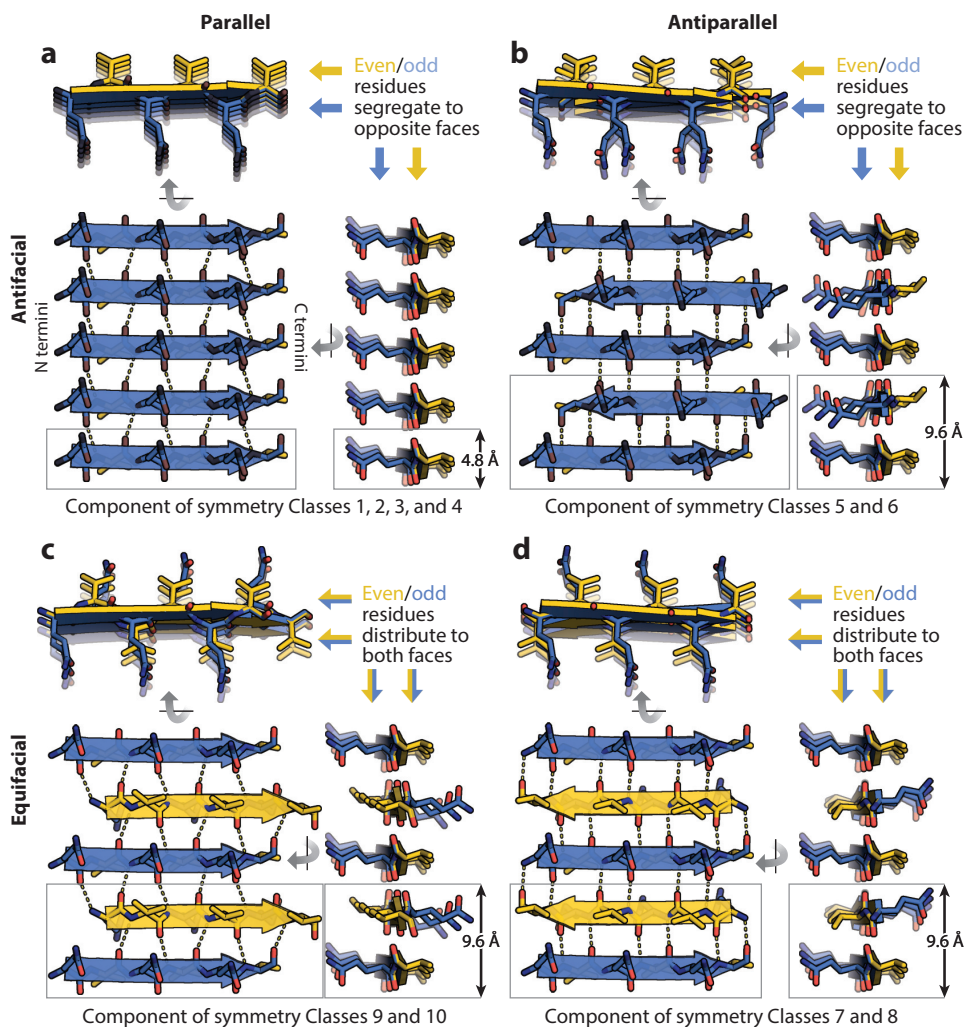


**Figure 3**

The four basic  $\beta$ -sheet symmetry patterns. All strands are illustrated using the same hypothetical 6-mer sequence, 1-QVQVQV-6. Odd-numbered residues are colored blue; even-numbered residues are colored yellow. (a,c) Parallel sheets can be either antifacial or equifacial. (b,d) Likewise, antiparallel sheets can be either antifacial or equifacial. Only the parallel antifacial pattern has a translational repeat distance along the fibril direction of 4.8 Å. The remaining three patterns have a repeat distance of 9.6 Å.

strands align with opposite polarities, yielding both N termini and C termini on both edges (i.e., the arrows point in opposite directions in **Figure 3b,d**). In amyloid, another type of polarity may also develop—between opposite faces of a sheet. This distinction arises from the fact that successive residues protrude from opposite faces of a strand. Antifacial sheets are defined when strands align to yield one face composed entirely of even-numbered residues and the opposite face composed entirely of odd-numbered residues (**Figure 3a,b**). Conversely, equifacial sheets are defined when strands align to yield both faces composed of both even- and odd-numbered residues (**Figure 3c,d**).



**In-register:** a sheet is defined as in-register if its translational repeat direction is perpendicular to the strand direction

These two dichotomies in sheet polarity, parallel versus antiparallel and antifacial versus equifacial, combine to give four patterns of sheet symmetry. That is, parallel sheets can be either antifacial (**Figure 3a**) or equifacial (**Figure 3c**); likewise, antiparallel sheets can be either antifacial (**Figure 3b**) or equifacial (**Figure 3d**). All these symmetries have been crystallographically observed except for parallel-equifacial, which may have two energetic disadvantages to its formation. First, parallel sheets are slightly less favorable than antiparallel sheets (disregarding the influence of side chains) due to differences in hydrogen-bonding geometry (63). Second, equifacial symmetry reduces the chance that like-residues will stack into ladders, as they can in antifacial parallel sheets. Furthermore, an unlimited number of more complex symmetry patterns are possible in  $\beta$ -sheets, involving additional symmetry elements and periodicities of more than one or two strands (i.e., longer than 4.8 Å or 9.6 Å); however, evidence of their existence has not yet been found.

### Ten Symmetry Classes

The four basic  $\beta$ -sheet patterns defined above are each capable of self-pairing to form cross- $\beta$  spines; in total, ten distinct spine symmetry classes can be enumerated. These classes are distinguished by the particular sheet pattern and the symmetry operation that relates the pair of sheets. For example, parallel-antifacial sheets give rise to four of the ten spine symmetry classes (**Figure 4**). These are distinguished by whether the sheets are related by (a) a 2-fold symmetry axis oriented along the fibril axis (Class 1), (b) pure translation (Class 2), (c) a 2-fold parallel to the strand direction (Class 3), or (d) a 2-fold normal to the sheet face (Class 4). These operations produce recognizable and distinctive features in the spine. For example, Classes 1 and 3 are distinguished by face-to-face packing, and Classes 2 and 4 are distinguished by face-to-back packing. Similarly, Classes 3 and 4 are distinguished by an exchange of up and down directions between sheets (up-down), whereas Classes 1 and 2 do not exchange up and down directions (up-up). Each of the remaining three  $\beta$ -sheet patterns likewise gives rise to distinct symmetry classes (two each), bringing the total to ten classes.

The particular symmetry adopted by an amyloid spine may help explain its characteristic fibril morphology or biophysical properties. For example, if hydrophilic and hydrophobic residues alternate in sequence, antifacial sheets may display amphipathic character. Such sheets may readily pair as protofibrils through their hydrophobic surfaces (Classes 1, 3, or 5), leaving the hydrophilic surface to negotiate weak associations between protofibrils. Conversely, amphipathicity is unachievable for equifacial sheets, whose opposite faces must be symmetrically identical (Classes 7–10). Such sheets may associate with no discrete termination point, perhaps yielding fibrils with variable ribbon-like dimensions. Similarly, spines with face-to-back symmetry (Classes 2, 4, and 6) may also pack with no discrete termination point.

### Strand Registration

In addition to the symmetry relationships described above, variations may arise from differences in registration between strands within a sheet. A strong bias for strands to align in-register is evident in the structures of the three best-determined, full-length amyloid fibrils known to date: A $\beta$ ,  $\alpha$ -synuclein ( $\alpha$ -syn), and HET-s (64–67). In-register is defined in parallel-antifacial  $\beta$ -sheets when backbone amide and carbonyl groups of residue  $n$  are hydrogen bonded to carbonyl and amide groups of residues  $n - 1$  and  $n + 1$  of a neighboring chain, respectively. That is, identical residues from neighboring chains stack along the fibril axis. Such ladder-type stacking can be energetically favorable for uncharged residues. Furthermore, the sheets are highly kinked in the three cited structures; these kinks are made possible by sharp turns, often enabled by glycine.

Eisenberg • Sawaya

3.12



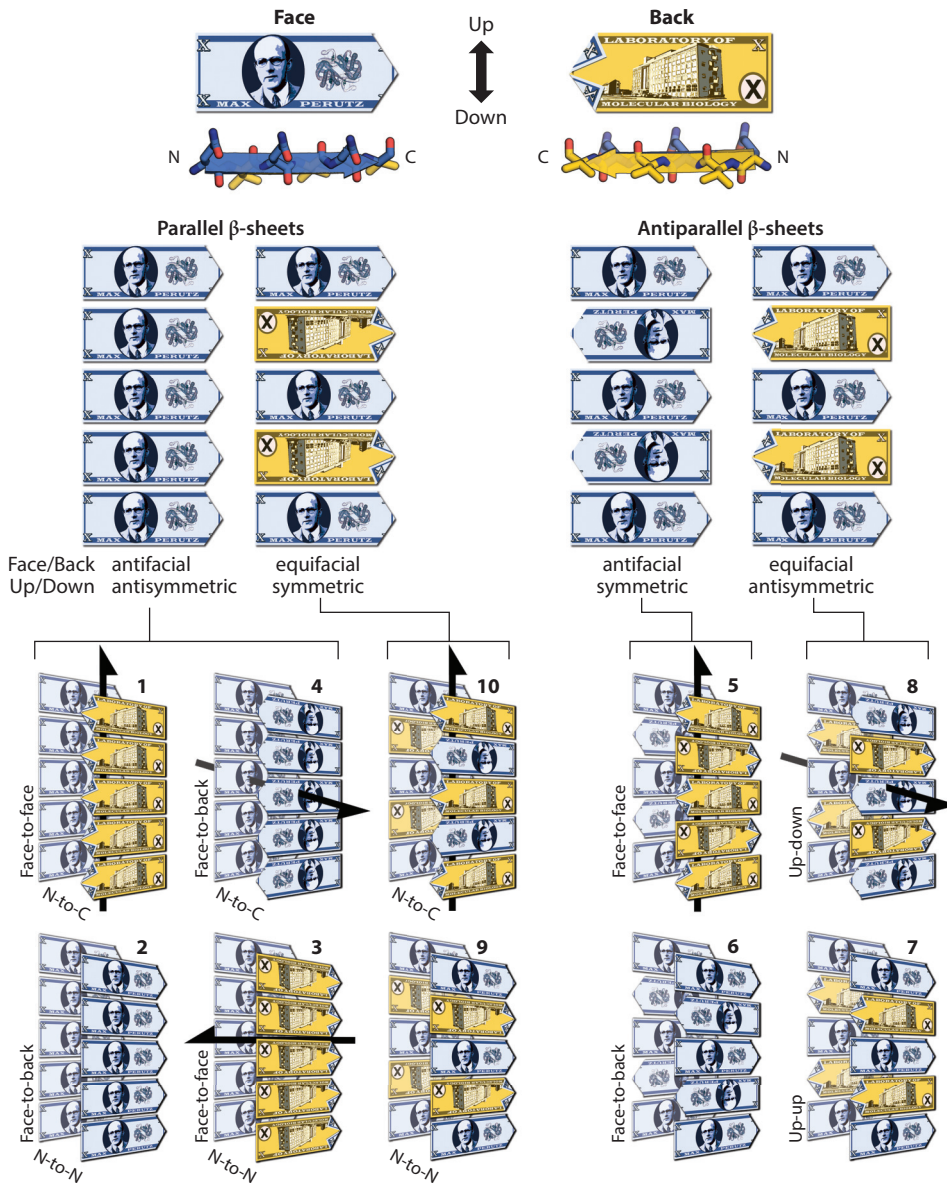


**Figure 4**

The ten amyloid symmetry classes of homo-steric zipper amyloid spines, illustrated with the fictitious Max Perutz bank note. At the top, notice that a  $\beta$ -strand has an N terminus, a C terminus, a front face, a back face, an up edge, and a down edge. Single-bladed arrows signify  $2_1$  symmetry axes, meaning that the two sheets are related by a  $180^\circ$  rotation about the arrow and a translation along the arrow of one-half the repeat distance between Max Perutz bank notes.



**Out-of-register:**

a sheet is defined as out-of-register if its translational repeat direction is not orthogonal to the strand direction

**ssNMR:** solid-state nuclear magnetic resonance

Such a high degree of kinking would be improbable for out-of-register sheets, because lack of registration would destroy the alignment of these special kink-assisting residues.

Differences in registry are also possible for antiparallel sheets and parallel-equifacial sheets; however, the definition of registry requires some adaptation because, in these types of sheets, neighboring strands adopt different orientations, eliminating the possibility that all residues in the sheet stack with identical residues. We adopt a broader view of registry, applicable to all patterns of  $\beta$ -sheets. We define a sheet to be in-register when a line drawn between any pair of identically oriented chains lies perpendicular to the strand direction (50, 68). Such a line would not be perpendicular to the strand direction in out-of-register sheets. When flattened out, the four edges of any in-register sheet would be a rectangle, whereas any out-of-register sheet would be a nonrectangular parallelogram (**Figure 2**). Furthermore, because the translational repeat vector is tilted away from the strand direction, a split in the meridional reflection is expected in fiber diffraction patterns. Just such a split is observed in the electron diffraction pattern of nanotubes composed of  $A\beta_{16-22}$  and attributed to out-of-register antiparallel sheets (69). An alternate definition for registry in antiparallel sheets was adopted by Liang et al. (70). Their definition of in-register and out-of-register antiparallel sheets corresponds to what we describe as antiparallel-antifacial and equifacial sheets, respectively.

## THE SEQUENCE DEPENDENCE OF AMYLOID FIBRILS

As far as is known, each type of amyloid fibril is a regular aggregate of a single protein. Antibody staining has failed to reveal fibril spines built from two or more distinct proteins. Also, fibrils of a protein, or even fibril-forming segments of a protein, can readily seed (accelerate) the growth from monomers into fibrils of the same protein or of proteins of similar sequence (48). As the sequences diverge, seeding becomes less effective and unrelated proteins are ineffective for seeding (71). Furthermore, dominant mutations in a disease-related protein can lead to enhanced fibril formation of that one protein and increased severity of disease. All of these observations suggest that formation of amyloid fibrils is dependent on the amino acid sequence of the fibril-forming protein. That is, the hydrogen bonding of the amide groups of the protein backbone is not the only force that favors aggregation; interactions of the side chains also contribute.

The structures of the amyloid spines illustrated in **Figure 2** show how certain amino acid sequences favor aggregation: These sequences are self-complementary. When arranged in a  $\beta$ -sheet, they bond tightly to a  $\beta$ -sheet formed from identical sequences. Such self-complementary interaction offers one explanation for why amyloid fibrils are formed from only one type of protein. The pattern of self-complementary bonding of the pair of interacting sheets can be extended by adding monomers to the tips of the fibrils. This process of seeding is expected to be most effective when the sequence of the added molecule matches that of the molecules already in the fibril.

Non-self-complementary sequences can also form tightly mating interfaces between sheets. Recent structures of amyloid fibrils determined by ssNMR have revealed hetero-steric zippers in fibrils of  $A\beta$ ,  $\alpha$ -syn, and HET-s. We describe such hetero-steric zippers in the following sections.

## STRUCTURAL STUDIES OF SOME PATHOGENIC AMYLOID FIBRILS

### $\beta$ -Amyloid<sub>1-40</sub>

The plaques first observed in a diseased brain by Alois Alzheimer have been found to be composed mainly of a peptide of varying length between 38–43 residues known as  $\beta$ -amyloid ( $A\beta$ ). The two most prevalent lengths are  $A\beta_{1-40}$  and the more cytotoxic  $A\beta_{1-42}$ . Three models of fibrils

Eisenberg • Sawaya

3:14



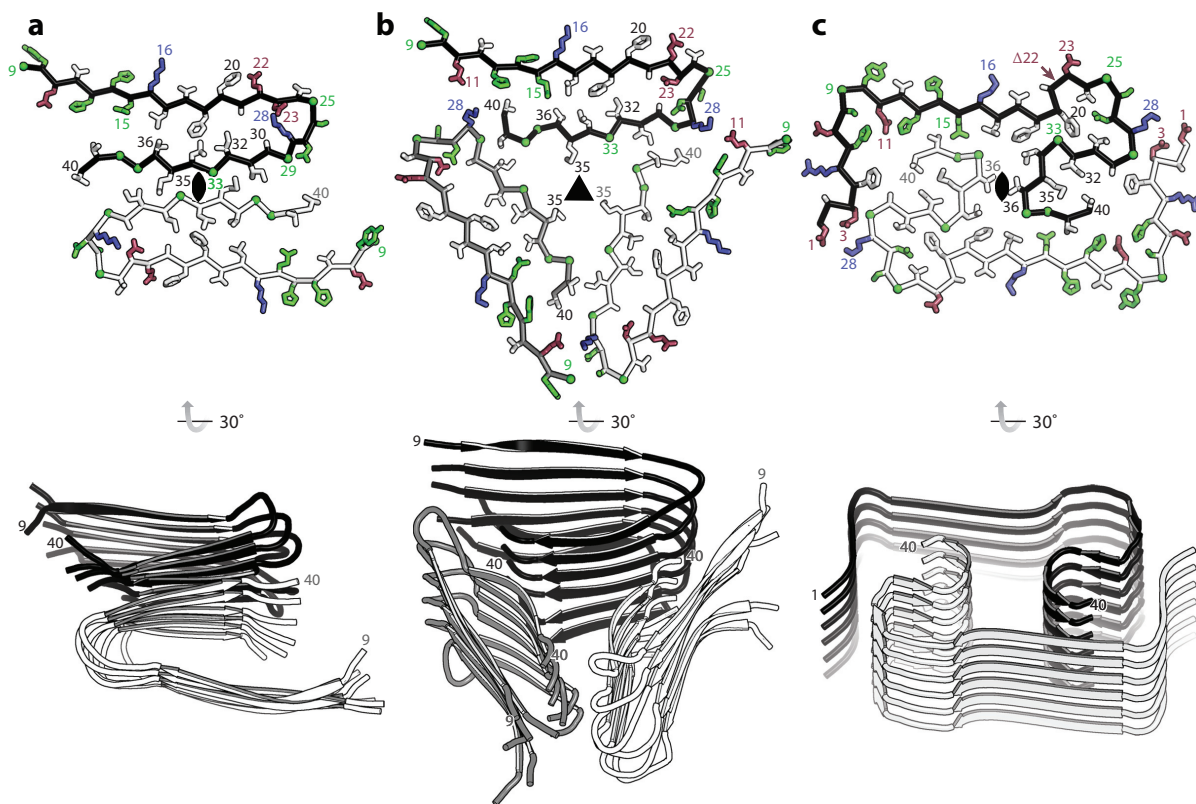


**Figure 5**

Solid-state nuclear magnetic resonance–determined models of three polymorphs of amyloid fibrils formed by  $A\beta_{1-40}$ . The upper row gives views down the protofilament axes; the lower row gives views of six layers more nearly perpendicular to the protofilament axes. All three polymorphs contain parallel, in-register  $\beta$ -sheets. (a) Striated ribbons (70) grown under agitating conditions. Each molecule forms a U shape, with residues 30–40 of the two molecules forming a homo-steric zipper at an approximate 2-fold axis of symmetry. Residues 23–29 form bends, with residue D23 salt bridging to K28, and residues 10–20 form the extended strands farthest from the 2-fold axis. Each U may be considered a hetero-steric zipper in which two different  $\beta$ -sheets form a tight, dry interface. Protein Data Bank (PDB) code 2LMN. (b) Twisted pairs grown under quiescent conditions form a similar U-shaped structure, but in this case three molecules are related by an approximate 3-fold axis of symmetry near residue 35 (72). PDB code 2LMQ. (c)  $A\beta_{1-40}$ , bearing the Osaka mutation ( $\Delta 22$ ) (73). The two sharply kinked molecules of the protofilament meet at a 2-fold axis of symmetry near residue 36. The molecule makes sharp kinks at glycine residues. In all three models, glycines and apolar residues are green, positively charged residues are blue, and negatively charged residues are red.

of  $A\beta_{1-40}$  determined by ssNMR are shown in **Figure 5** (72–74). Although all are of  $A\beta_{1-40}$ , these polymorphs appear distinctly different. The fibril shown in **Figure 5a** was grown under agitating conditions, whereas the fibril in **Figure 5b** was grown under quiescent conditions. The most obvious difference is that the protofilament of **Figure 5a** is a dimer with approximate 2-fold symmetry, and **Figure 5b** is a trimer with approximate 3-fold symmetry. In both, the  $A\beta_{1-40}$  molecules are U shaped, with residues 10–22 in one arm of the U and residues 30–40 in the other arm. In both, the  $\beta$ -sheets are parallel and in-register, with each  $A\beta_{1-40}$  molecule sitting exactly above the molecule below it in the sheet.

A third ssNMR structure for  $A\beta_{1-40}$  is shown in **Figure 5c**, quite different from the others. As in **Figure 5a**, the protofilament is a dimer, with  $\beta$ -sheets parallel and in-register, but instead of

a U shape, the structure is highly kinked. This is the structure of the so-called Osaka mutation, 33 $\Delta$ , associated with early onset Alzheimer disease, but the authors state that “the overall fold is thus, in principle, also accessible to the wild-type A $\beta_{1-40}$ ” as well as the other early onset mutations found at positions 21–23 (75, p. 334). Clearly A $\beta_{1-40}$  is capable of forming several polymorphic amyloid fibrils.

### $\beta$ -Amyloid<sub>1-42</sub>

The structure of A $\beta_{1-42}$  has been eagerly awaited because it is the major A $\beta$  species in the amyloid plaques observed in the brains of Alzheimer patients. Also, the additional isoleucine and alanine at its C terminus cause it to aggregate more rapidly than A $\beta_{1-40}$ . Two independent ss-NMR determinations arrived at essentially the same model, having near-atomic resolution (64, 65). The protofilament consists of stacks of two nearly flat, highly kinked molecules of A $\beta_{1-42}$ , which are related by a 2-fold axis. Each molecule turns sharply at each of three Gly residues, forming the shape of two horseshoes or an inverted S (**Figure 6**). Each molecule is hydrogen bonded to identical molecules both above and below it in the protofilament. Two groups of apolar residues form two hydrophobic clusters in the interior, and polar side chains extend from the protofilament surface, accessible to solvent. Four extended segments of each molecule are  $\beta$ -strands that stack into  $\beta$ -sheets that run the entire length of the protofilament. Notice that neighboring  $\beta$ -strands are closely packed, forming hetero-steric zippers (**Figure 6c**). A homosteric zipper is formed where the two molecules meet at the 2-fold axis. Notice that this homosteric zipper is formed by two noncontiguous sequence segments from each molecule (**Figure 6d**). The inverted S shape of the monomer had been determined the year before, also by ssNMR (76).

Reactivity with antibodies suggests that this polymorphic form of A $\beta_{1-42}$  is relevant to Alzheimer disease (64). These fibrils are positive in dot blots with antibodies that bind intracellular deposits and senile plaques from the brains of Alzheimer disease patients, and they are negative for antibodies that are not able to detect intracellular deposits and senile plaques from human Alzheimer patients.

How this polymorph exerts its toxic effect is not known, but there are hints. Residue alanine 42, absent in A $\beta_{1-40}$ , forms a hydrophobic stripe together with residue valine 40 along the exterior of the protofilament. It has been speculated that this stripe may enhance secondary nucleation of a toxic species (65). Secondary nucleation is distinguished from primary nucleation, in which fibrils elongate by the addition of monomers to the ends. In secondary nucleation, monomers are nucleated into oligomeric aggregates by interaction with exterior faces of the  $\beta$ -sheets (22). The resulting oligomers may be toxic to cells. A second hint about the origin of toxicity also comes from the structure. The segment running from residue 16 to 23 forms a bulge in the structure (**Figure 6a**), which harbors residues found mutated in several early onset forms of Alzheimer disease. Conceivably this bulge binds to a receptor that triggers disease.

As for A $\beta_{1-40}$ , there appear to be at least two amyloid polymorphs of A $\beta_{1-42}$ . **Figure 6g,b** shows a cryo-EM reconstruction from information extracted from 29 fibrils of another fibril form of A $\beta_{1-42}$ . The protofilament appears to consist of two long  $\beta$ -sheets that twist around each other. The cross section reveals two extended molecules of A $\beta_{1-42}$  with the poorly ordered N terminus apparently executing a U turn. The overall resolution of the reconstruction is approximately 7 Å, increasing to approximately 5 Å near the 2-fold axis. Using antibodies, the authors established the N-terminal region of the molecule (77).



3.16 Eisenberg • Sawaya

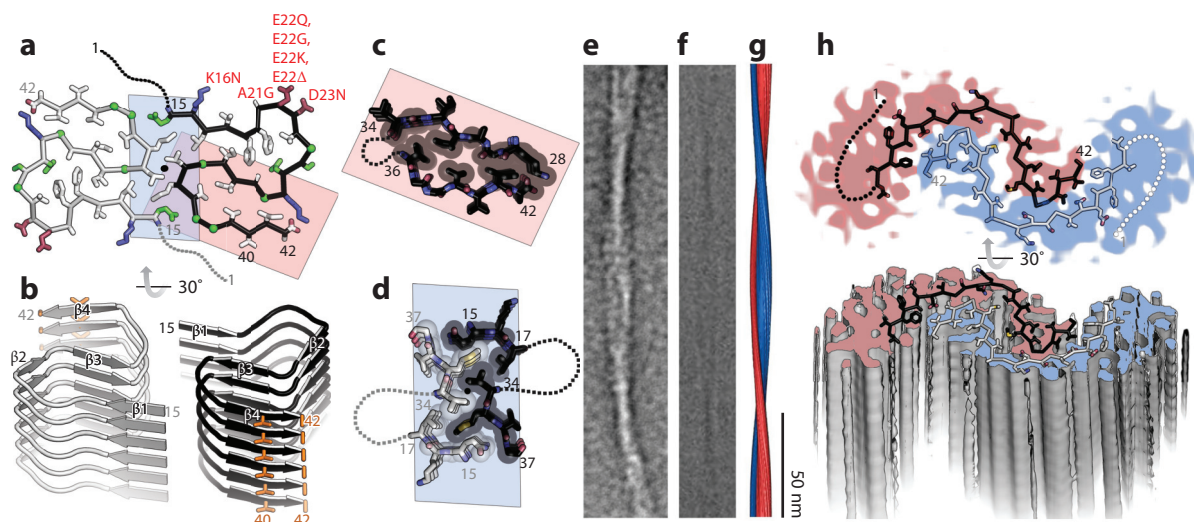


**Figure 6**

Structures of two polymorphs of  $A\beta_{1-42}$ . (*a-d*) Solid-state nuclear magnetic resonance (ssNMR) structure (62, 63). (*a*) This view down the protofilament axis shows the two relatively flat molecules of the protofilament bound closely to each other around the 2-fold axis (*black circle*). Each molecule has the shape of a double horseshoe, enabled by kinks in the backbone at the glycine residues. The poorly ordered N termini of residues 1–14 are represented by dotted lines. Notice the bulge at the upper right containing the mutations (labeled) found in families with severe or early onset Alzheimer disease. Glycines and polar residues are green, positively charged residues are blue, and negatively charged residues are red. Apolar residues are colored black or white. (*b*) The structure from panel *a* tilted by  $30^\circ$  to show six of the thousands of layers of the protofilament. A hydrophobic stripe defined by residues 40 and 42 (*orange*) may enhance secondary nucleation of a toxic species. Notice the four  $\beta$ -sheets. (*c*) Enlargement of the pink rectangle from panel *a* to show the hetero-steric zipper formed by the horseshoe of residues 28–42. (*d*) Enlargement of the blue rectangle from panel *a* to show the homo-steric zipper at the interface of the two molecules. Notice that each molecule contributes two noncontiguous segments to the zipper, residues 15–17 and 34–37. Dotted lines indicate intervening sequences. (*e-b*) Cryo-electron microscopy (cryo-EM) reconstruction of a second polymorph of  $A\beta_{1-42}$  (99). (*e*) Transmission electron micrograph of a heavy metal-stained protofilament. (*f*) Cryo-EM image of a protofilament. (*g*) 3D reconstruction of the protofilament. (*h*) Cross section of the reconstruction, with a model of residues superimposed. The dotted lines are estimates of the path of the poorly ordered N-terminal segment. Panels *e-g* modified from Reference 77 with permission.

### $\alpha$ -Synuclein

$\alpha$ -Syn, a protein of 140 residues, is the main protein component of Lewy bodies, the defining histological feature of Parkinson disease (78). Evidence that aggregated  $\alpha$ -syn is a molecular cause of Parkinson disease includes the observation that families afflicted with inherited disease bear mutations in  $\alpha$ -syn and show abundant Lewy bodies (79). The middle domain, residues 61–95, is termed NAC. NAC has long been implicated in  $\alpha$ -syn aggregation, and in particular, residues 68–78, termed NACore, have been found to be essential for fibril formation (80, 81). Electron diffraction yielded atomic-resolution structures of fibrils of both NACore and of a second segment termed PreNAC, situated in the sequence just before NAC (**Figure 7**) (82). NACore forms a tight homo-steric zipper ( $Sc = 0.72$ ), which may explain its rapid formation of amyloid fibrils and perhaps its strong cytotoxicity.

ssNMR has determined a largely ordered structure for residues 44–97 of  $\alpha$ -syn (**Figure 7a,b**) (66). As with  $A\beta$ , the molecule is essentially flat, but there is only one molecule per layer of the protofilament (i.e., no rotational symmetry and hence no homo-steric zipper). The layers are held together by the hydrogen bonds of the parallel, in-register  $\beta$ -sheets and a glutamine

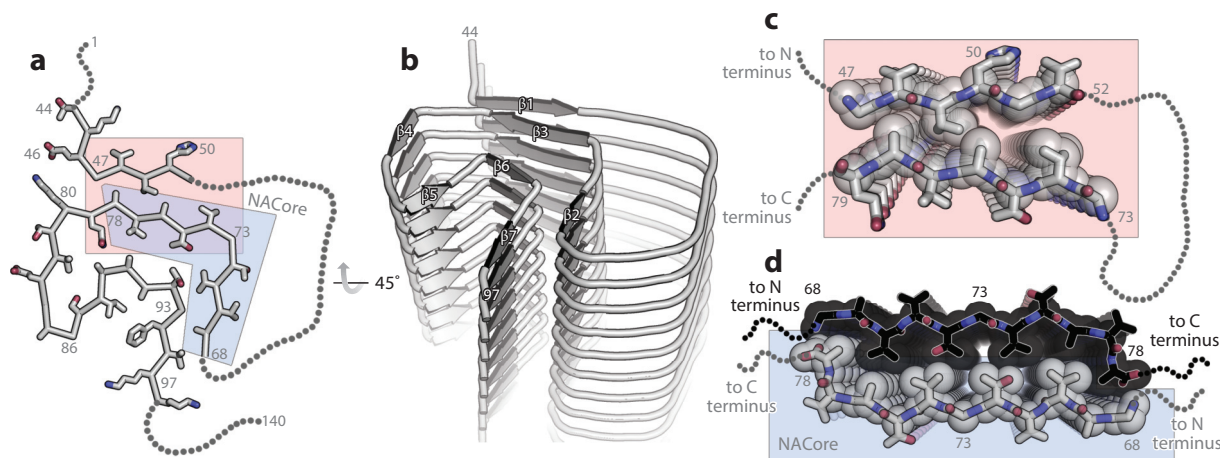


**Figure 7**

Structure of  $\alpha$ -synuclein segments. (a,b) Solid-state nuclear magnetic resonance structure of residues 44–97, which encompasses the full NAC (residues 61–95) (64). The parallel, in-register layers of molecules kink sharply, taking the path of a Greek key. Seven short  $\beta$ -strands are within each molecule. Only one stack of molecules composes each protofilament, which excludes the possibility of homo-steric zippers. However, there are three short hetero-steric zippers, one of which is highlighted in a pink box and magnified in panel c. The L-shaped blue box highlights an 11-residue segment termed the NACore, which was determined by crystallographic methods (80) and is detailed in panel d. The NACore forms a homo-steric zipper in the crystal and lacks the kink at Gly73.

ladder along the fibril axis. As for  $A\beta$ , the chain is highly kinked with several short hetero-steric zippers, including two formed by residues of NACore. Measurements of the mass-per-unit length of the fibril are consistent with one molecule per layer of the protofilament. Consequently, the protofilament is narrow, only approximately 5 nm in width, the same width of  $\alpha$ -syn fibrils isolated from the substantia nigra of Parkinson disease patients. In fact, the fibrils for this study produced  $\alpha$ -syn inclusions in hippocampal neurons (66), validating its relevance to disease.

### STRUCTURAL BASIS OF POLYMORPHS AND STRAINS

Unlike globular proteins, for which a given amino acid sequence folds into a unique 3D structure, a given protein in the amyloid state can assume several different cross- $\beta$  structures—a situation termed polymorphism. Examples of amyloid polymorphism are illustrated in **Figure 8**.

Prion strains are phenomena related to amyloid polymorphs. In microorganisms, strains are defined as phenotypic variants encoded by variant gene sequences. Amyloid or prion strains are defined as phenotypic variants encoded by the same protein sequence, which assumes variant protein conformations (83). Because the phenotype is transmitted from cell to cell, or from one generation of an organism to the next, the protein conformation encoding the phenotype must be stable enough to endure the process of transmission. Whereas such conformations as the R and T states of hemoglobin are not separated by an energy barrier high enough to encode separate strains, the polymorphs of amyloid fibrils are separated by large energy barriers, compared with thermal energy, and thus seem to offer the required persistence for encoding strains. The question then arises: What are possible molecular mechanisms capable of encoding conformational strains?

Crystal structures of steric zipper spines of amyloid fibrils suggest possible answers. **Figure 8** shows pairs of steric zippers, both members of the pair having the same sequence but with different structures. The structures differ in the packing of the two sheets of the zipper, termed packing

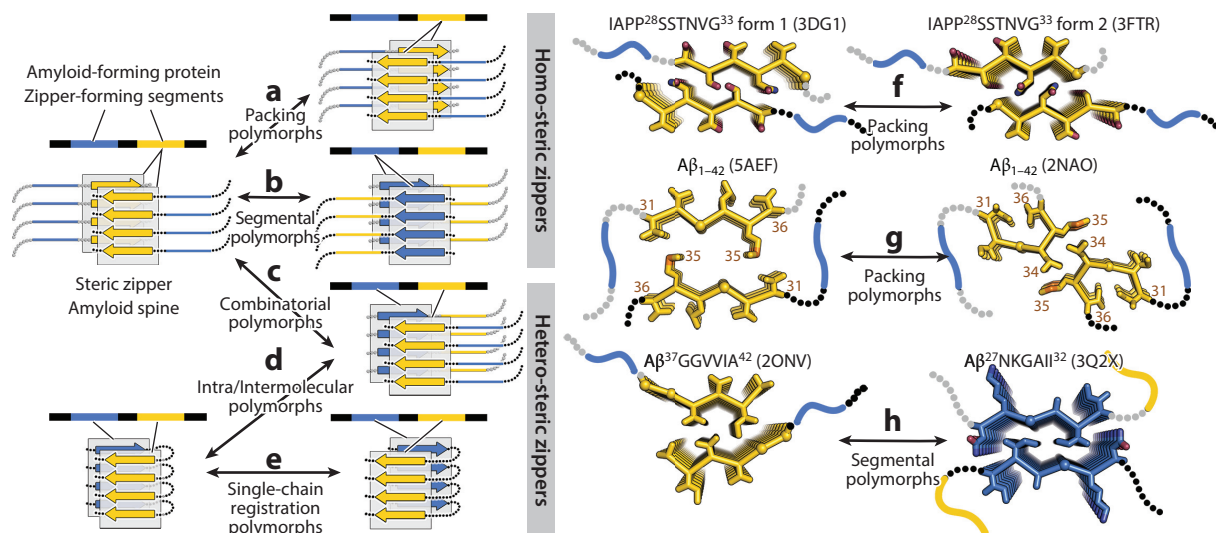


**Figure 8**

Molecular basis for amyloid polymorphism. (a–e) Schematic diagram of how several amyloid polymorphs can arise from a protein with two segments of high aggregation propensity (yellow and blue segments). (a) Packing polymorphs can arise if identical segments can pack into different steric zippers, for example with shifts in registration between sheets. (b) Segmental polymorphs can arise if two different segments can each pack into a steric zipper. (c) Combinatorial polymorphs can arise if a segment can form both a homo-steric and a hetero-steric zipper. (d,e) The possibility of hetero-steric zippers increases the potential for polymorphism. (f–h) Atomic-resolution structures of steric zipper pairs illustrate molecular structures that enable amyloid polymorphism. (f) A pair of packing polymorphic steric zippers formed by segment SSTNVG from islet amyloid polypeptide (IAPP). (g) A pair of packing polymorphs of steric zippers formed by segments of  $\beta$ -amyloid ( $A\beta_{1-42}$ ). (h) A pair of polymorphic steric zippers of segments from  $A\beta$ .

polymorphism (42). The corresponding fibrils thus display different patterns of side chains on their surfaces and might be expected to encode different amyloid phenotypes. A second type of polymorphism is segmental polymorphism, which arises because most amyloid-forming proteins contain several potential steric zipper-forming segments. For example, prion protein (PrP) contains at least five segments that form steric zippers (84). Each of these segments can serve as the spine of a polymorphic amyloid fibril, as illustrated in **Figure 8b**. A third type of polymorphism is enabled by the formation of hetero-steric zippers (**Figure 8c,d,e**). Hetero-steric zippers form between two different segments of the protein, adding still other potential polymorphs. With all three of these modes of amyloid polymorphism possible, the number of strains encoded by a given amyloid-forming protein could be large. In fact, a large number of strains are known for PrP (85).

### Structural Basis of Seeding and Prion-Like Spreading

The biological significance of amyloid seeding has long been appreciated (86). Monomers of amyloid-forming proteins do not readily form fibrils even when they are more concentrated in solution than the critical concentration necessary for fibril formation. The high-energy barrier on the pathway to a fibril is the formation of a fibril nucleus, to which monomers can add, thereby growing the fibril. When a nucleus, in the form of a fibril seed, is introduced into the solution, the energy barrier is bypassed and fibrils grow rapidly. Amyloid seeding is thought to be the basis for prion-like spreading of amyloid fibrils from cell to cell in tissues and from animal to animal in PrP infection and hence for disease transmission (87–89).



Examination of steric zipper spines of amyloid fibrils gives insight into the high-energy barrier for formation of amyloid nuclei (4). The minimum template that establishes the pattern of intermolecular bonding in a steric zipper requires at least three and perhaps four molecules of the segment, because the pattern of hydrogen bonding within either of the two  $\beta$ -sheets requires two molecules. In addition, the pattern of side chain interdigitation between the two mating  $\beta$ -sheets requires at least one molecule from the second sheet to form the zipper-like interface with the two molecules of the first sheet. For this nucleus or seed to form, the three or four participating molecules must all be spatially close and must open to expose their zipper-forming segment at the same instant. This seems a rare event. However, once the seed is formed, only one molecule at a time needs to open and add to the nucleus for the fibril to grow. This is a much more common event. For this reason, fibril growth is far faster than fibril nucleation, and seeding greatly accelerates fibril growth. Amyloid fibrils can apparently migrate from cell to cell and can act as seeds in the recipient cell, provided monomer concentration of the same protein is sufficiently high in the recipient cell (90, 91).

### STRUCTURAL STUDIES OF AMYLOID OLIGOMERS

Although the defining feature of amyloid-related conditions is their association with fibrils, studies from many laboratories have suggested that in at least some diseases, the molecular agents are lower-molecular-weight entities of the same proteins, termed amyloid oligomers (92–95). These oligomers are transient species that appear during the conversion of monomers to stable fibrils. Attempts to characterize the sizes, structures, and properties of these entities have been frustrated by their ensemble of shapes and stoichiometries and their tendency to convert rapidly into fibrils. Among points of contention are the number of molecules in amyloid oligomers, with various experiments detecting some with hundreds of molecules and others with as few as two. The suggestion that amyloid oligomers have common structural features regardless of constituent amyloid protein was based on the production of an antibody termed A11 that was reported to bind to all oligomers (92). Because of the biochemical challenges, few proposals have been made for the structures of amyloid oligomers at the molecular level.

A possible model for an amyloid oligomer was offered by the crystal structure of a segment of the amyloid-forming protein  $\alpha$ B-crystallin (96). An 11-residue segment with sequence KVKVLGDVIEV was crystallized and its structure determined by X-ray methods. The structure (**Figure 9a**) is a cylindrical  $\beta$ -sheet, unlike the steric zipper spines of amyloid fibrils. The six  $\beta$ -strands are antiparallel and out-of-register, in contrast to the in-register structure of most amyloid fibril structures. A 25-residue, tandem-repeat version of this sequence gives essentially the same structure and is recognized by the A11 antibody, which reportedly binds to amyloid oligomers but not monomers or fibrils. This cylindrical structure, or cylindrin, is somewhat cytotoxic and thus seems to fulfill the definition of an amyloid oligomer as a low-molecular-weight molecular species of an amyloid-forming sequence that is cytotoxic and recognized by the A11 antibody. Also supporting the hypothesis that antiparallel, out-of-register  $\beta$ -sheets may be associated with cytotoxicity is the structure of an out-of-register fibril found to be toxic to cells (49).

A structural feature of out-of-register  $\beta$ -sheets is consistent with the transient nature of amyloid oligomers: Because the  $\beta$ -strands are out-of-register sheets, each strand has dangling hydrogen bonds, resulting in weaker interactions than the in-register strands of most amyloid aggregates. These weaker interactions may explain why amyloid oligomers rapidly transform into amyloid fibrils.

A very different atomic model proposed for oligomers of  $A\beta_{1-42}$  emerged from biophysical studies of a preparation of oligomers with molecular weights in the range of  $80,000 \pm 20,000$  Da,

Eisenberg • Sawaya

3.20



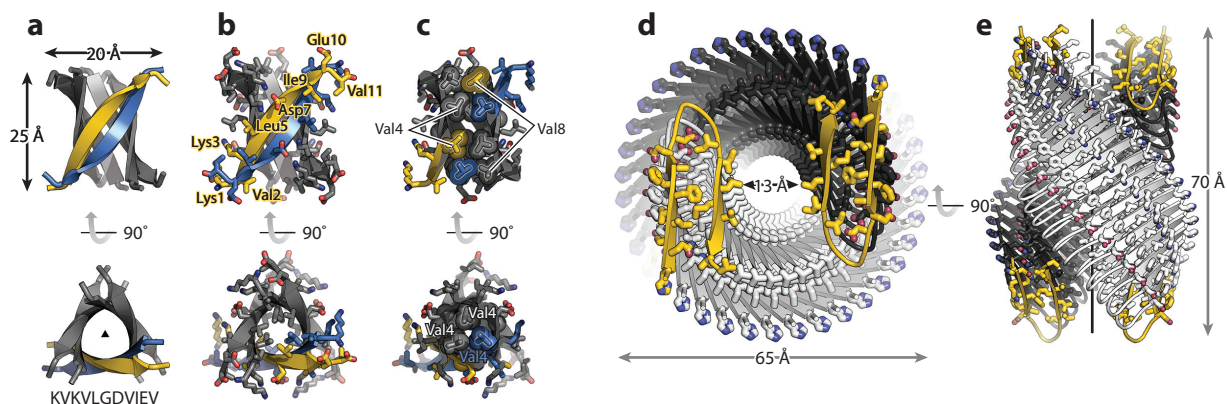


**Figure 9**

Speculative models for amyloid oligomers. (*a–c*) Cylindrin is composed of 3 antiparallel pairs of  $\beta$ -strands, 11 residues each, with sequence KVKVLGDVIEV from  $\alpha$ B-crystallin. (*a*) Cartoon representation of cylindrin oligomer. The oligomer is D3 symmetric, meaning it contains one 3-fold rotational symmetry axis and, perpendicular to it, three 2-fold rotational symmetry axes. The top panels show a view down one of the 2-fold rotation axis of symmetry. The bottom panels show a view down the 3-fold rotation axis of symmetry. (*b*) The outside surface of cylindrin is composed of both charged and nonpolar residues. (*c*) The inside is composed entirely of nonpolar residues, Val4, Gly6, and Val8. Yellow and blue colors distinguish opposite strand directions. (*d*) Cross sections of cylindrin show that the inside of the oligomer is tightly packed with hydrophobic side chains. (*d,e*) A model for a toxic amyloid  $\beta$  fibrillar oligomer (TABFO) comprising 38 molecules of  $\beta$ -amyloid<sub>1–40</sub>. Each molecule has a U shape. The molecules at the ends of the TABFO are in yellow. The model comprises two short segments of cross- $\beta$  fibrils wrapped around each other. Capping protomers are colored yellow.

approximately 15–24 molecules (97). These oligomers are  $\beta$ -sheet rich and judged to be antiparallel by Fourier transform infrared analysis. They display a powder X-ray diffraction pattern unlike those of  $\beta$ -helices, stacked  $\beta$ -strands, or porins. Rather, the diffraction pattern is consistent with that of helical  $\beta$ -sheet pairs wrapped around each other to form a superhelix (**Figure 9b**). That is, the model is of two twisting steric zippers forming a double helix of four  $\beta$ -sheets. The central open pore can have varying diameters, depending on the pitch of the helix.

A related model for oligomers of A $\beta$ <sub>1–42</sub> was proposed on the basis of studies by site-directed spin labeling and electron paramagnetic resonance (98). In this model, each A $\beta$  molecule forms a  $\beta$ -sheet with three antiparallel strands, and four of these are arranged head-to-tail. Four such sheets are packed face-to-back.

## SUMMARY AND GAPS IN OUR UNDERSTANDING OF AMYLOID STRUCTURES AT THE MOLECULAR LEVEL

The powerful structural tools of cryo-EM, ssNMR, and X-ray and electron diffraction have begun to uncover the fundamental architectural elements of amyloid fibrils. We now know that closely mating pairs of  $\beta$ -sheets, in both homo-steric and hetero-steric zippers, stabilize amyloid fibrils. We know that lines of polarized hydrogen bonds between layers and hydrophobic interactions also contribute to the great stability of these many-layered structures. Whereas antiparallel sheets are found in some amyloid fibrils, parallel in-register  $\beta$ -sheets seem to be more common and enable the added energetic bonding of ladders of stacked side chains running down the surfaces of fibrils. Despite these advances, we lack knowledge of the molecular-level architecture of complex amyloid fibrils, which comprise multiple protofilaments.

The variety of amyloid structures available at present define the possible modes of assembly and symmetries of  $\beta$ -sheets. They also offer insights into the molecular basis of amyloid polymorphism. They suggest, but do not prove, that prion-like strains are carried by polymorphic fibrils that seed the same polymorph.

Despite these advances we lack firm understanding of the link between amyloid structure and disease. Why are numerous diseases associated with morphologically similar, but molecularly distinct, fibrils? To what extent are amyloid aggregates the cause of diseases? Despite much effort, uncertainties remain about the disease-causing entities: Are they fibrils or small oligomeric aggregates, or both? What do amyloid oligomers share in common? Is there firm evidence that amyloid oligomers are in all cases distinct from small fibrils? Why for some proteins are oligomers more toxic than fibrils on a weight basis? Are oligomers more toxic than fibrils on a mole basis? (18). For amyloid diseases of the central nervous system, is there a common mechanism of toxicity, and if so, what is it? Will inhibition of fibril formation halt disease progression either for systemic or neurodegenerative amyloid diseases?

Some eight decades have passed since Astbury's pioneering study on amyloid. With the powerful tools of structural, molecular, and cellular biology available today, we can hope that many of the remaining crucial questions about amyloid structure and action can be answered within one more decade.

#### SUMMARY POINTS

1. Many proteins aggregate into amyloid fibrils, some associated with diseases, others with biological functions in bacteria, fungi, and animals, and others upon denaturation.
2. Amyloid fibrils are built from tens of thousands of molecules that stack extended  $\beta$ -strands into  $\beta$ -sheet spines.
3. The common structural elements of amyloid fibrils are closely mating  $\beta$ -sheets with tight interfaces that are generally devoid of water. These are termed steric zippers.
4. Amyloid fibrils are often more stable than other protein assemblies. Contributing factors to stability include steric zippers between both identical (homo-steric zippers) and non-identical (hetero-steric zippers)  $\beta$ -sheets, polarized hydrogen bonds between layers of  $\beta$ -strands, release of previously bound water molecules upon formation of steric zippers, and ladders of interacting side chains.
5. Because of the tight interaction (surface-to-surface complementarity) of  $\beta$ -sheets in steric zippers, the formation of amyloid fibrils is determined in part by the amino acid sequence.
6. Ten specific symmetries are possible for the packing of identical  $\beta$ -sheet pairs in homo-steric zippers.
7. In contrast with globular proteins, a given protein in the amyloid state can aggregate into several distinctly different polymorphic structures.
8. Smaller aggregates of fibril-forming proteins, termed oligomers, containing tens rather than tens of thousands of identical molecules, may be the toxic agents in some amyloid diseases.

#### DISCLOSURE STATEMENT

D.S.E. is cofounder and chair of the scientific advisory board of ADRx Inc.

*Eisenberg • Sawaya*



## ACKNOWLEDGMENTS

We thank with great gratitude our numerous coworkers and collaborators who have worked with us to understand the structural biology of amyloid as well as the agencies who have supported our work, including Howard Hughes Medical Institute, National Institutes of Health, and US Department of Energy. D.S.E. is grateful to the Vallee Foundation for a visiting professorship and to his hosts Drs. Alan Fersht and Michel Goedert for valuable discussions.

## LITERATURE CITED

1. Sipe JD, Benson MD, Buxbaum JN, Ikeda S, Merlini G, et al. 2014. Nomenclature 2014: amyloid fibril proteins and clinical classification of the amyloidosis. *Amyloid* 21(4):221–24
2. Astbury WT, Dickinson S, Bailey K. 1935. The X-ray interpretation of denaturation and the structure of the seed globulins. *Biochem. J.* 29(10):2351–60.1
3. Pauling L, Corey RB. 1951. Configurations of polypeptide chains with favored orientations around single bonds: two new pleated sheets. *PNAS* 37(11):729–40
4. Nelson R, Sawaya MR, Balbirnie M, Madsen AØ, Riekel C, et al. 2005. Structure of the cross- $\beta$  spine of amyloid-like fibrils. *Nature* 435(7043):773–78
5. Cohen AS, Calkins E. 1959. Electron microscopic observations on a fibrous component in amyloid of diverse origins. *Nature* 183(4669):1202–3
6. Eanes ED, Glenner GG. 1968. X-ray diffraction studies on amyloid filaments. *J. Histochem. Cytochem.* 16(11):673–77
7. Sunde M, Serpell LC, Bartlam M, Fraser PE, Pepys MB, Blake CC. 1997. Common core structure of amyloid fibrils by synchrotron X-ray diffraction. *J. Mol. Biol.* 273(3):729–39
8. Hardy J, Selkoe DJ. 2002. The amyloid hypothesis of Alzheimer's disease: progress and problems on the road to therapeutics. *Science* 297(5580):353–56
9. Goedert M, Spillantini MG. 2006. A century of Alzheimer's disease. *Science* 314(5800):777–81
10. Perrin RJ, Fagan AM, Holtzman DM. 2009. Multimodal techniques for diagnosis and prognosis of Alzheimer's disease. *Nature* 461(7266):916–22
11. Katzman R, Terry R, DeTeresa R, Brown T, Davies P, et al. 1988. Clinical, pathological, and neurochemical changes in dementia: a subgroup with preserved mental status and numerous neocortical plaques. *Ann. Neurol.* 23(2):138–44
12. Harper JD, Wong SS, Lieber CM, Lansbury PT. 1997. Observation of metastable A $\beta$  amyloid protofibrils by atomic force microscopy. *Chem. Biol.* 4(2):119–25
13. Walsh DM, Lomakin A, Benedek GB, Condron MM, Teplow DB. 1997. Amyloid  $\beta$ -protein fibrillogenesis: detection of a protofibrillar intermediate. *J. Biol. Chem.* 272(35):22364–72
14. Nag S, Sarkar B, Chandrakesan M, Abhyanakar R, Bhowmik D, et al. 2013. A folding transition underlies the emergence of membrane affinity in amyloid- $\beta$ . *Phys. Chem. Chem. Phys.* 15(44):19129–33
15. Benilova I, Karran E, De Strooper B. 2012. The toxic A $\beta$  oligomer and Alzheimer's disease: an emperor in need of clothes. *Nat. Neurosci.* 15(3):349–57
16. Lorenzo A, Yankner BA. 1994.  $\beta$ -Amyloid neurotoxicity requires fibril formation and is inhibited by Congo red. *PNAS* 91(25):12243–47
17. Winner B, Jappelli R, Maji SK, Desplats PA, Boyer L, et al. 2011. In vivo demonstration that  $\alpha$ -synuclein oligomers are toxic. *PNAS* 108(10):4194–99
18. Pieri L, Madiona K, Bousset L, Melki R. 2012. Fibrillar  $\alpha$ -synuclein and Huntingtin exon 1 assemblies are toxic to the cells. *Biophys. J.* 102(12):2894–905
19. Abedini A, Plesner A, Cao P, Ridgway Z, Zhang J, et al. 2016. Time-resolved studies define the nature of toxic IAPP intermediates, providing insight for anti-amyloidosis therapeutics. *eLife* 5:e12977
20. Ikenoue T, Lee Y-H, Kardos J, Saiki M, Yagi H, et al. 2014. Cold denaturation of  $\alpha$ -synuclein amyloid fibrils. *Angew. Chem. Int. Ed. Engl.* 53(30):7799–804



21. Buell AK, Dobson CM, Knowles TPJ. 2014. The physical chemistry of the amyloid phenomenon: thermodynamics and kinetics of filamentous protein aggregation. *Essays Biochem.* 56:11–39
22. Gustavsson A, Engström U, Westermark P. 1991. Normal transthyretin and synthetic transthyretin fragments form amyloid-like fibrils in vitro. *Biochem. Biophys. Res. Commun.* 175(3):1159–64
23. Colon W, Kelly JW. 1992. Partial denaturation of transthyretin is sufficient for amyloid fibril formation in vitro. *Biochemistry* 31(36):8654–60
24. Booth DR, Sunde M, Bellotti V, Robinson CV, Hutchinson WL, et al. 1997. Instability, unfolding and aggregation of human lysozyme variants underlying amyloid fibrillogenesis. *Nature* 385(6619):787–93
25. Guijarro JI, Sunde M, Jones JA, Campbell ID, Dobson CM. 1998. Amyloid fibril formation by an SH3 domain. *PNAS* 95(8):4224–28
26. Fändrich M, Fletcher MA, Dobson CM. 2001. Amyloid fibrils from muscle myoglobin. *Nature* 410(6825):165–66
27. Fändrich M, Dobson CM. 2002. The behaviour of polyamino acids reveals an inverse side chain effect in amyloid structure formation. *EMBO J.* 21(21):5682–90
28. Goldschmidt L, Teng PK, Riek R, Eisenberg D. 2010. Identifying the amyloids, proteins capable of forming amyloid-like fibrils. *PNAS* 107(8):3487–92
29. Otzen D. 2010. Functional amyloid: turning swords into plowshares. *Prion* 4(4):256–64
30. Pham CLL, Kwan AH, Sunde M. 2014. Functional amyloid: widespread in nature, diverse in purpose. *Essays Biochem.* 56:207–19
31. Chapman MR, Robinson LS, Pinkner JS, Roth R, Heuser J, et al. 2002. Role of *Escherichia coli* curli operons in directing amyloid fiber formation. *Science* 295(5556):851–55
32. Maji SK, Perrin MH, Sawaya MR, Jessberger S, Vadodaria K, et al. 2009. Functional amyloids as natural storage of peptide hormones in pituitary secretory granules. *Science* 325(5938):328–32
33. Fowler DM, Koulov AV, Alory-Jost C, Marks MS, Balch WE, Kelly JW. 2006. Functional amyloid formation within mammalian tissue. *PLoS Biol.* 4(1):e6
34. Kato M, Han TW, Xie S, Shi K, Du X, et al. 2012. Cell-free formation of RNA granules: Low complexity sequence domains form dynamic fibers within hydrogels. *Cell* 149(4):753–67
35. Si K, Lindquist S, Kandel ER. 2003. A neuronal isoform of the *Aphysia* CPEB has prion-like properties. *Cell* 115(7):879–91
36. Knowles TPJ, Buehler MJ. 2011. Nanomechanics of functional and pathological amyloid materials. *Nat. Nanotechnol.* 6(8):469–79
37. Li D, Furukawa H, Deng H, Liu C, Yaghi OM, Eisenberg DS. 2014. Designed amyloid fibers as materials for selective carbon dioxide capture. *PNAS* 111(1):191–96
38. Balbirnie M, Grothe R, Eisenberg DS. 2001. An amyloid-forming peptide from the yeast prion Sup35 reveals a dehydrated  $\beta$ -sheet structure for amyloid. *PNAS* 98(5):2375–80
39. Bowie JU, Lüthy R, Eisenberg D. 1991. A method to identify protein sequences that fold into a known three-dimensional structure. *Science* 253(5016):164–70
40. Thompson MJ, Sievers SA, Karanicolas J, Ivanova MI, Baker D, Eisenberg D. 2006. The 3D profile method for identifying fibril-forming segments of proteins. *PNAS* 103(11):4074–78
41. Sawaya MR, Sambashivan S, Nelson R, Ivanova MI, Sievers SA, et al. 2007. Atomic structures of amyloid cross- $\beta$  spines reveal varied steric zippers. *Nature* 447(7143):453–57
42. Wiltzius JJW, Landau M, Nelson R, Sawaya MR, Apostol MI, et al. 2009. Molecular mechanisms for protein-encoded inheritance. *Nat. Struct. Mol. Biol.* 16(9):973–78
43. Wiltzius JJW, Sievers SA, Sawaya MR, Eisenberg D. 2009. Atomic structures of IAPP (amylin) fusions suggest a mechanism for fibrillation and the role of insulin in the process. *Protein Sci.* 18(7):1521–30
44. Apostol MI, Sawaya MR, Cascio D, Eisenberg D. 2010. Crystallographic studies of prion protein (PrP) segments suggest how structural changes encoded by polymorphism at residue 129 modulate susceptibility to human prion disease. *J. Biol. Chem.* 285(39):29671–75
45. Apostol MI, Wiltzius JJW, Sawaya MR, Cascio D, Eisenberg D. 2011. Atomic structures suggest determinants of transmission barriers in mammalian prion disease. *Biochemistry* 50(13):2456–63

3:24 Eisenberg • Sawaya



46. Landau M, Sawaya MR, Faull KF, Laganowsky A, Jiang L, et al. 2011. Towards a pharmacophore for amyloid. *PLoS Biol.* 9(6):e1001080
47. Colletier J-P, Laganowsky A, Landau M, Zhao M, Soriaga AB, et al. 2011. Molecular basis for amyloid- $\beta$  polymorphism. *PNAS* 108(41):16938–43
48. Ivanova MI, Sievers SA, Guenther EL, Johnson LM, Winkler DD, et al. 2014. Aggregation-triggering segments of SOD1 fibril formation support a common pathway for familial and sporadic ALS. *PNAS* 111(1):197–201
49. Liu C, Zhao M, Jiang L, Cheng P-N, Park J, et al. 2012. Out-of-register  $\beta$ -sheets suggest a pathway to toxic amyloid aggregates. *PNAS* 109(51):20913–18
50. Soriaga AB, Sangwan S, Macdonald R, Sawaya MR, Eisenberg D. 2016. Crystal structures of IAPP amyloidogenic segments reveal a novel packing motif of out-of-register beta sheets. *J. Phys. Chem. B* 120(26):5810–16
51. Soragni A, Janzen DM, Johnson LM, Lindgren AG, Thai-Quynh Nguyen A, et al. 2016. A designed inhibitor of p53 aggregation rescues p53 tumor suppression in ovarian carcinomas. *Cancer Cell* 29(1):90–103
52. Roland BP, Kodali R, Mishra R, Wetzel R. 2013. A serendipitous survey of prediction algorithms for amyloidogenicity. *Biopolymers* 100(6):780–89
53. Tycko R. 2011. Solid-state NMR studies of amyloid fibril structure. *Annu. Rev. Phys. Chem.* 62:279–99
54. Paravastu AK, Qahwash I, Leapman RD, Meredith SC, Tycko R. 2009. Seeded growth of  $\beta$ -amyloid fibrils from Alzheimer's brain-derived fibrils produces a distinct fibril structure. *PNAS* 106(18):7443–48
55. Bai X, McMullan G, Scheres SHW. 2015. How cryo-EM is revolutionizing structural biology. *Trends Biochem. Sci.* 40(1):49–57
56. Tsemekhman K, Goldschmidt L, Eisenberg D, Baker D. 2007. Cooperative hydrogen bonding in amyloid formation. *Protein Sci.* 16(4):761–64
57. Lawrence MC, Colman PM. 1993. Shape complementarity at protein/protein interfaces. *J. Mol. Biol.* 234(4):946–50
58. Stroud JC. 2013. The zipper groups of the amyloid state of proteins. *Acta Crystallogr. Sect. D* 69(Pt 4):540–45
59. White HE, Hodgkinson JL, Jahn TR, Cohen-Krausz S, Gosal WS, et al. 2009. Globular tetramers of  $\beta_2$ -microglobulin assemble into elaborate amyloid fibrils. *J. Mol. Biol.* 389(1):48–57
60. Fitzpatrick AWP, Debelouchina GT, Bayro MJ, Clare DK, Caporini MA, et al. 2013. Atomic structure and hierarchical assembly of a cross- $\beta$  amyloid fibril. *PNAS* 110(14):5468–73
61. Jiménez JL, Nettleton EJ, Bouchard M, Robinson CV, Dobson CM, Saibil HR. 2002. The protofilament structure of insulin amyloid fibrils. *PNAS* 99(14):9196–9201
62. Jiménez JL, Guijarro JJ, Orlova E, Zurdo J, Dobson CM, et al. 1999. Cryo-electron microscopy structure of an SH3 amyloid fibril and model of the molecular packing. *EMBO J.* 18(4):815–21
63. Chou KC, Pottle M, Némethy G, Ueda Y, Scheraga HA. 1982. Structure of  $\beta$ -sheets: origin of the right-handed twist and of the increased stability of antiparallel over parallel sheets. *J. Mol. Biol.* 162(1):89–112
64. Wälti MA, Ravotti F, Arai H, Glabe CG, Wall JS, et al. 2016. Atomic-resolution structure of a disease-relevant A $\beta$ (1–42) amyloid fibril. *PNAS* 113(34):e4976–84
65. Colvin MT, Silvers R, Ni QZ, Can TV, Sergeyev IV, et al. 2016. Atomic resolution structure of monomorphous A $\beta$ <sub>42</sub> amyloid fibrils. *J. Am. Chem. Soc.* 138(30):9663–74
66. Tuttle MD, Comellas G, Nieuwkoop AJ, Covell DJ, Berthold DA, et al. 2016. Solid-state NMR structure of a pathogenic fibril of full-length human  $\alpha$ -synuclein. *Nat. Struct. Mol. Biol.* 23(5):409–15
67. Van Melckebeke H, Wasmer C, Lange A, Ab E, Loquet A, et al. 2010. Atomic-resolution three-dimensional structure of HET-s(218–289) amyloid fibrils by solid-state NMR spectroscopy. *J. Am. Chem. Soc.* 132(39):13765–75
68. Liu C, Sawaya MR, Eisenberg D. 2011. B<sub>2</sub>-microglobulin forms three-dimensional domain-swapped amyloid fibrils with disulfide linkages. *Nat. Struct. Mol. Biol.* 18(1):49–55
69. Mehta AK, Lu K, Childers WS, Liang Y, Dublin SN, et al. 2008. Facial symmetry in protein self-assembly. *J. Am. Chem. Soc.* 130(30):9829–35
70. Liang C, Ni R, Smith JE, Childers WS, Mehta AK, Lynn DG. 2014. Kinetic intermediates in amyloid assembly. *J. Am. Chem. Soc.* 136(43):15146–49



71. O'Nuallain B, Williams AD, Westermark P, Wetzel R. 2004. Seeding specificity in amyloid growth induced by heterologous fibrils. *J. Biol. Chem.* 279(17):17490–99
72. Petkova AT, Leapman RD, Guo Z, Yau W-M, Mattson MP, Tycko R. 2005. Self-propagating, molecular-level polymorphism in Alzheimer's  $\beta$ -amyloid fibrils. *Science* 307(5707):262–65
73. Petkova AT, Yau W-M, Tycko R. 2006. Experimental constraints on quaternary structure in Alzheimer's  $\beta$ -amyloid fibrils. *Biochemistry* 45(2):498–512
74. Paravastu AK, Leapman RD, Yau W-M, Tycko R. 2008. Molecular structural basis for polymorphism in Alzheimer's  $\beta$ -amyloid fibrils. *PNAS* 105(47):18349–54
75. Schütz AK, Vagt T, Huber M, Ovchinnikova OY, Cadalbert R, et al. 2015. Atomic-resolution three-dimensional structure of amyloid  $\beta$  fibrils bearing the Osaka mutation. *Angew. Chem. Int. Ed. Engl.* 54(1):331–35
76. Xiao Y, Ma B, McElheny D, Parthasarathy S, Long F, et al. 2015. A $\beta$ (1–42) fibril structure illuminates self-recognition and replication of amyloid in Alzheimer's disease. *Nat Struct Mol Biol.* 22(6):499–505
77. Schmidt M, Rohou A, Lasker K, Yadav JK, Schiene-Fischer C, et al. 2015. Peptide dimer structure in an A $\beta$ (1–42) fibril visualized with cryo-EM. *PNAS* 112(38):11858–63
78. Spillantini MG, Schmidt ML, Lee VM, Trojanowski JQ, Jakes R, Goedert M. 1997.  $\alpha$ -Synuclein in Lewy bodies. *Nature* 388(6645):839–40
79. Polymeropoulos MH, Lavedan C, Leroy E, Ide SE, Dehejia A, et al. 1997. Mutation in the  $\alpha$ -synuclein gene identified in families with Parkinson's disease. *Science* 276(5321):2045–47
80. Bodles AM, Guthrie DJ, Greer B, Irvine GB. 2001. Identification of the region of non-A $\beta$  component (NAC) of Alzheimer's disease amyloid responsible for its aggregation and toxicity. *J. Neurochem.* 78(2):384–95
81. Giasson BI, Murray IV, Trojanowski JQ, Lee VM. 2001. A hydrophobic stretch of 12 amino acid residues in the middle of  $\alpha$ -synuclein is essential for filament assembly. *J. Biol. Chem.* 276(4):2380–86
82. Rodriguez JA, Ivanova MI, Sawaya MR, Cascio D, Reyes FE, et al. 2015. Structure of the toxic core of  $\alpha$ -synuclein from invisible crystals. *Nature* 525(7570):486–90
83. Tanaka M, Chien P, Naber N, Cooke R, Weissman JS. 2004. Conformational variations in an infectious protein determine prion strain differences. *Nature* 428(6980):323–28
84. Rodriguez JA, Jiang L, Eisenberg D. 2016. *Toward the Atomic Structure of PrP<sup>Sc</sup>*. Cold Spring Harb., NY: Cold Spring Harbor Lab. In press
85. Safar J, Wille H, Itri V, Groth D, Serban H, et al. 1998. Eight prion strains have PrP<sup>Sc</sup> molecules with different conformations. *Nat. Med.* 4(10):1157–65
86. Jarrett JT, Lansbury PT. 1993. Seeding “one-dimensional crystallization” of amyloid: A pathogenic mechanism in Alzheimer's disease and scrapie? *Cell* 73(6):1055–58
87. Prusiner SB. 2012. A unifying role for prions in neurodegenerative diseases. *Science* 336(6088):1511–13
88. Aguzzi A, Rajendran L. 2009. The transcellular spread of cytosolic amyloids, prions, and prionoids. *Neuron* 64(6):783–90
89. Luk KC, Kehm V, Carroll J, Zhang B, O'Brien P, et al. 2012. Pathological  $\alpha$ -synuclein transmission initiates Parkinson-like neurodegeneration in nontransgenic mice. *Science* 338(6109):949–53
90. Kfoury N, Holmes BB, Jiang H, Holtzman DM, Diamond MI. 2012. Trans-cellular propagation of tau aggregation by fibrillar species. *J. Biol. Chem.* 287(23):19440–51
91. Eisele YS, Obermüller U, Heilbronner G, Baumann F, Kaeser SA, et al. 2010. Peripherally applied A $\beta$ -containing inoculates induce cerebral  $\beta$ -amyloidosis. *Science* 330(6006):980–82
92. Kaye R, Head E, Thompson JL, McIntire TM, Milton SC, et al. 2003. Common structure of soluble amyloid oligomers implies common mechanism of pathogenesis. *Science* 300(5618):486–89
93. Fändrich M. 2012. Oligomeric intermediates in amyloid formation: structure determination and mechanisms of toxicity. *J. Mol. Biol.* 421(4–5):427–40
94. Haass C, Selkoe DJ. 2007. Soluble protein oligomers in neurodegeneration: lessons from the Alzheimer's amyloid  $\beta$ -peptide. *Nat. Rev. Mol. Cell Biol.* 8(2):101–12
95. Silveira JR, Raymond GJ, Hughson AG, Race RE, Sim VL, et al. 2005. The most infectious prion protein particles. *Nature* 437(7056):257–61
96. Laganowsky A, Liu C, Sawaya MR, Whitelegge JP, Park J, et al. 2012. Atomic view of a toxic amyloid small oligomer. *Science* 335(6073):1228–31

3:26

Eisenberg • Sawaya



97. Stroud JC, Liu C, Teng PK, Eisenberg D. 2012. Toxic fibrillar oligomers of amyloid- $\beta$  have cross- $\beta$  structure. *PNAS* 109(20):7717–22
98. Gu L, Liu C, Stroud JC, Ngo S, Jiang L, Guo Z. 2014. Antiparallel triple-strand architecture for prefibrillar A $\beta$ 42 oligomers. *J. Biol. Chem.* 289(39):27300–313
99. Kishimoto A, Hasegawa K, Suzuki H, Taguchi H, Namba K, Yoshida M. 2004.  $\beta$ -Helix is a likely core structure of yeast prion Sup35 amyloid fibers. *Biochem. Biophys. Res. Commun.* 315(3):739–45

